Neural Networks 62 (2015) 73–82

Contents lists available at ScienceDirect

Neural Networks

journal homepage: www.elsevier.com/locate/neunet

2015 Special Issue

Computational model of visual hallucination in dementia with Lewy bodies

Hiromichi Tsukada [a,*], Hiroshi Fujii [b], Kazuyuki Aihara [c], Ichiro Tsuda [a,d]

[a] Research Institute for Electronic Science, Hokkaido University, Sapporo 060-0812, Japan
[b] Department of Intelligent Systems, Kyoto Sangyo University, Kyoto 603-8555, Japan
[c] Institute of Industrial Science, The University of Tokyo, Tokyo 153-8505, Japan
[d] Research Center for Integrative Mathematics (RCIM), Hokkaido University, Sapporo 060-0812, Japan

ARTICLE INFO

Article history:
Available online 16 September 2014

Keywords:
Dementia with Lewy bodies
Visual hallucination
Conduction disturbance
Top-down facilitation
Object identity
Scene gist

ABSTRACT

Patients with dementia with Lewy bodies (DLB) frequently experience visual hallucination (VH), which has been aptly described as people seeing things that are not there. The distinctive character of VH in DLB necessitates a new theory of visual cognition. We have conducted a series of studies with the aim to understand the mechanism of this dysfunction of the cognitive system. We have proposed that if we view the disease from the internal mechanism of neurocognitive processes, and if also take into consideration recent experimental data on conduction abnormality, at least some of the symptoms can be understood within the framework of network (or disconnection) syndromes.

This paper describes the problem from a computational aspect and tries to determine whether conduction disturbances in a computational model can in fact produce a "computational" hallucination under appropriate assumptions.

1. Introduction

Patients with dementia with Lewy bodies (DLB) frequently experience visual hallucination (VH), which Collerton, Perry, and McKeith (2005) aptly described as the phenomenon where "people see things that are not there".

The distinctive character of VH in DLB appears at first glance to challenge the conventional theory of visual cognition. In DLB, hallucinatory images are mostly single entities, for example, an integrated image of a human or animal, and appear at the center of attention. The persistence of VH images is typically on the order of minutes but can sometimes be seconds or even hours, depending on the patient (Mosimann et al., 2006). What is most distinctive is that the image appears on a normal background scene, and at only the center of attention, a non-existing image is additionally superimposed. Also, the figure is consistent with the context and setting in which it appears (Collerton et al., 2005; McKeith et al., 2005; Perry & Perry, 1995). Hence, some cognitive functions appear intact, whereas others are hallucinatory.

We have conducted a series of studies aiming to understand the core mechanism of this dysfunction of the cognitive system, and to make experimentally testable predictions that may lead to a plausible etiology.

We have proposed that if we view the disease from the internal mechanism of neurocognitive processes, and if we also take into consideration recent experimental data on conduction abnormality (Catani & de Schotten, 2012; Catani & ffytche, 2005), at least some of the symptoms can be understood within the framework of network (or disconnection) syndromes, that is, hodotopical dysfunctions[1] (Catani & ffytche, 2005). VH in DLB may have homology with some of other cognitive dysfunctions, including the conduction aphasia reported by Geshwind (1965), Rykhlevskaia, Uddin, Kondos, and Menon (2009); for a much earlier account, see Lichtheim (1885).

In VH of DLB, the prefrontal cortex (PFC) might be disturbed, but without intrinsic pathology; hence, one or more of the fasciculi connecting the PFC with the visual or temporal areas might

* Corresponding author. Tel.: +81 0 117 06 2413; fax: +81 0 117 06 2413.
E-mail address: tsukada@es.hokudai.ac.jp (H. Tsukada).

http://dx.doi.org/10.1016/j.neunet.2014.09.001
0893-6080/

[1] In Greek, "topos" means place, while "hodos" means road or path. Thus, by topological and hodological dysfunction we refer, respectively, to dysfunction of the cortex itself and dysfunction related to connecting pathways, respectively. A hodotopic view thus refers to a hodological–topological point of view (ffytche, 2008), and we use the term *network* syndromes for such dysfunctions.

be damaged but other connections could remain intact (Goedert, Spillantini, Del Tredici, & Braak, 2013).

Recent imaging technology provides a means of experimentally studying the possible deficits (Catani & de Schotten, 2012) of connecting fasciculi. Further discussion of the pathophysiology of VH associated with DLB will be a focus of future studies.

The present study describes the problem of VH in DLB from a computational aspect, and seeks to determine whether conduction disturbances in our computational model can produce a "computational" hallucination under appropriate assumptions. The main part of this proposal was presented in Fujii, Tsukada, Tsuda, and Aihara (2014).

2. Orbitofrontal cortex triggers top-down facilitation

The content and character of VH in DLB primarily reflect the nature of visual processing (Collerton et al., 2005), and VH is a consequence of dysfunction of the normal visual cognitive system. Thus, understanding the brain mechanisms underlying normal object recognition is of crucial importance.

2.1. Standpoints

Understanding the neural mechanisms that underlie object recognition in both normal and dysfunctional states naturally leads us to the study of the PFC, in particular the ventrolateral PFC (VLPFC) and the orbitofrontal cortex (OFC), and the inferior temporal cortex (IT). In this regard the following statements provide the essence of our arguments.

First, our argument regarding the visual system is, in contrast to the previous conventional bottom-up view that relies on hierarchical processing, based on a top-down view of object recognitions (Bar, 2003, 2004, 2006; Fenske, Aminoff, Gronau, & Bar, 2006; Kveraga, Ghuman, & Bar, 2007). In fact, the central notion here is the top-down facilitation of the IT activity triggered by the PFC (Collerton, Dudley, & Mosimann, 2012). The facilitating signals to the IT are in the form of "bias" so that the IT can reactivate a detailed object representation. In this paper, we call this top-down signal an "index" so that it can encompass a range of top-down processes. However, the nature of this top-down "index" is currently a subject of debate.

In fact, the biasing signal that the PFC provides the IT may be an "initial guess" prediction about the *identity* of the object at the center of attention, as proposed by Bar and colleagues (Bar, 2003, 2004; Chaumon, Kveraga, Barrett, & Bar, 2013; Fenske et al., 2006; Kveraga et al., 2007). We have presumed this conceptualization in our computational implementation (Tsukada, Fujii, Tsuda, & Aihara, 2014).

Another conceptualization is that the nature of the index is *prior expectancy* for facilitating perception. In other words, the PFC provides the IT a set of *expectations* about possible interpretations of the input (Summerfield & Egner, 2009).

2.2. Integration of sensory information with memory

The PFC–VLPFC/OFC facilitates visual recognition by sending the IT top-down predictions about the identity of visual objects. To make a prediction the PFC needs to *integrate* incoming sensory information with *memory*. The part of the PFC that serves as the *memory system* for object-related semantic knowledge (OSK) is called the OSK network in the following.

In addition to information from the OSK network, the PFC itself relies on information from the visual stimulus at the center of attention (Chaumon et al., 2013) before an object is actually recognized. The information that the PFC receives in object recognition is rapidly extracted low-level information that has low spatial frequency, where associative information allows the formation of a predictive 'initial guess' about what objects are likely in the scene (Chaumon et al., 2013).

This rapid signal had once been supposed to be transmitted via a magnocellular pathway (Bar, 2003), but is now reasonably assumed to be transmitted via the inferior fronto-occipital fasciculus (iFOF), which can carry a wide range of information (Thiebaut de Schotten, Urbanski, Valabregue, Bayle, & Volle, 2012).

Such visual information (Bar, 2003) alone, however, cannot allow a unique guess on the identity of an object. *A string on a path in a dark forest could in fact be a snake*. Moreover, the context and setting in which an object appears, as well as expectancy and emotional state, may affect object identification.

Thus, the PFC itself receives, in addition to data from the *memory system* for object-related semantic knowledge, at least *three* major inputs for top-down indexing (see Figs. 1 and 2). The PFC receives rapidly arriving visual information on the external object via the direct pathway of the iFOF, and the two streams of input, namely, context- and expectancy-based reference information.

By what neural mechanisms does such facilitation take place? To our knowledge, few studies have examined this question. Here, we propose a conceptual mathematical model in an attempt to move in such a direction.

3. Prefrontal network for object-related semantic knowledge

The role of the PFC–VLPFC/OFC in object recognition is, first, to generate a guess on the identity of the object. In the present context, the PFC receives, among others, the following three main streams of projections to create such a guess on the identity:

I. Pathway I, as shown in Fig. 1, conveys rapid visual information, probably via iFOF from the occipital visual systems (such as V2/V4) (Bar, 2003; Fenske et al., 2006; Thiebaut de Schotten et al., 2012).
II. Pathway II conveys expectancy and emotional state via the OFC-IT-amygdala triad (Ghashghaei & Barbas, 2002).
III. Pathway III conveys contextual information as "the gist of the scene" from the retrosplenial cortex/parahippocampal cortex (Fenske et al., 2006).

A few notes are in order.

1. The early activity of the OFC, that is, the recognition-related activity in the OFC, precedes cortical activity in the IT (Bar, 2006).
2. It is suggested that gist-based contextual information transmitted via Pathway III is quickly processed (Kveraga et al., 2007).
3. IT neurons are activated by top-down signals even without bottom-up sensory signals (Tomita, Ohbayashi, Nakahara, Hasegawa, & Miyashita, 1999).

As stated above, part of the PFC (the OSK network) may be "*attuned to the associative content of visual information*" Chaumon et al. (2013), *and play the central role in* the indexing task. We assumed in the computational model that the OSK is a "super-imposed" hetero-associative network in which indices for facilitation are embedded. (For details, see Section 6.)

Signals transmitted via Pathway I serve as reference inputs, and those transmitted via Pathways II and III are regarded as contextual inputs. This output guess from the OSK network is then sent to the IT as a top-down trigger to facilitate activation of the image of the "seen" object (Bar, 2003). The question of how the IT can activate detailed object representation by means of the PFC bias index is explained in Section 5.

4. Core mechanism of recurrent complex visual hallucination: a working hypothesis

We have proposed the following working hypothesis on the core mechanism of recurrent complex VH (RCVH) (Fujii et al., 2014):

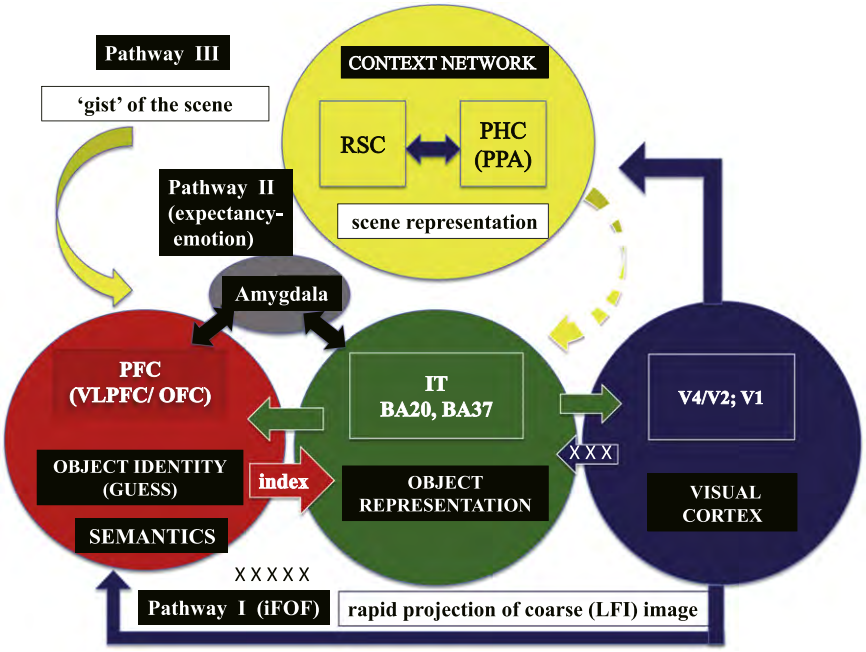

Fig. 1. Object recognition in normal case and with conduction disturbances. PPA is a part of the PHC, and is involved in the representation of scene (Epstein & Kanwisher, 1998). PPA is activated when human subjects view topographical images of scene such as landscapes, townscapes, or rooms. When the same area is damaged, patients cannot recognize the scene any more, but can see each object within the scene. We postulate that this is when attention is focused on it. Note, however, that the (semantic) identity and visual image of an object are not provided by the PPA, but by the PFC and the IT, respectively. Hence, while the topographical background image of a scene is furnished by the PPA, the foreground image (with identity) of each object is created by the interacting system of the PFC and the IT. The gist, or meaning of the scene is quickly analyzed by RSC, and sent to PFC via Pathway III (Biederman et al., 1974). The hypothesized pathways (marked as XXX) where conduction disturbances occur. Then, the index created by PFC is based on information via the remaining two pathways. The guess thus created may possibly be erroneous one, but still consistent with the context and the setting. Abbreviations: PFC (VLPFC/OFC), prefrontal cortex (ventrolateral PFC/orbitofrontal cortex); IT (BA20, BA37), inferior temporal cortex, fusiform gyrus; V4/V2; V1, visual cortices; RSC, retrosplenial cortex; PHC–PPA, parahippocampal complex—parahippocampal place area; OFC-IT-Amygdala TRIAD (Ghashghaei & Barbas, 2002); iFOF, inferior fronto-occipital fasciculus (a branch of the fasciculus connecting mono-synaptically the PFC (OFC) with the visual cortices Sarubbo et al., 2013).

Principal disorder: "Temporary conduction disturbance occurs somewhere along Pathway I".
Consequently, the OFC's prediction on object identity is made essentially on the basis of only the context input and the expectancy—emotion inputs.

In addition, we proposed that the following complementary disorder may occur at the same time:

Complementary disorder—"Conduction disturbance somewhere between the IT and the occipital visual cortex (V2/V4) occurs as well".

Because of the complementary disorder, it could happen that the IT is essentially blind to external objects at the center of attention, and that the IT loses the means to correct the hallucinatory index from the PFC in the process of PFC–IT interaction.

To sum up, we conclude that the PFC creates the "seed" of a particular hallucinatory image due to disturbance of information via Pathway I, and the IT implements this false index in a detailed image.

4.1. Pathophysiological bases related to the working hypothesis

Possible pathophysiology may be conduction disturbances along pathway I and other pathways (Court et al., 2001; Kiuchi et al., 2011; Ota et al., 2009; Reid, Sabbagh, Corey-Bloom, Tiraboschi, & Thal, 2000; Sanchez-Castaneda et al., 2010).

Alternative, but not exclusive, scenarios viewed from the internal neuro-cognitive mechanism presented in this paper could be possible: one is intrinsic pathology of the PFC, which may produce false indices (via pathways that are intact); and another is loss of attentional focus due to low level of cholinergic activity in the PFC (Kanamaru, Fujii, & Aihara, 2013). These might lead to similar hallucinatory symptom. We plan to conduct detailed studies on other possible scenarios in the future.

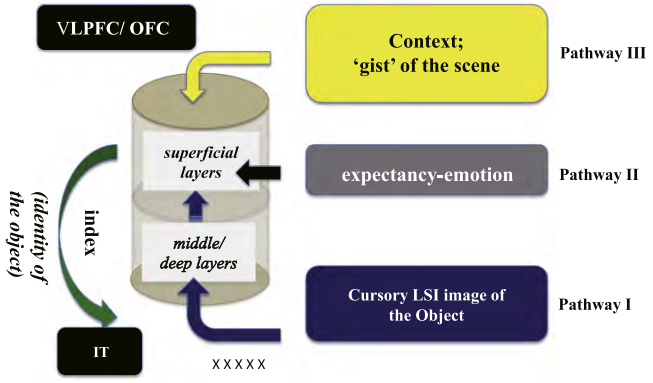

Fig. 2. PFC decision on the identity of an object is based on signals via three pathways. In normal object recognition, the PFC (VLPFC/ OFC) receives three streams of information via three Pathways, where Pathway I transmits rapid projections of LFI (coarse) information (Bar, 2003) on the object at the center of attention, Pathway II transmits expectancy and emotion via the OFC-IT-Amygdala Triad (Ghashghaei & Barbas, 2002), while Pathway III transmits contextual information, e.g., the gist (meaning) of the scene via the RSC. The PFC, integrating with memory (object-related semantic memory stored in the PFC), creates a prediction on the identity of the object at the center of attention. This prediction, called "index" in the present paper, will facilitate as a priming signal the reactivation of visual images of objects in the IT.

5. Object representation in the IT with top-down facilitation

The IT network receives an index from the PFC, and this biasing signal could activate object representation even without inputs from the visual cortices (Bar, 2004, 2006; Kastner & Ungerleider, 2001; Tomita et al., 1999). We postulate that this situation may occur in VH associated with DLB. We emphasize that IT neurons are activated by top-down signals without bottom-up sensory

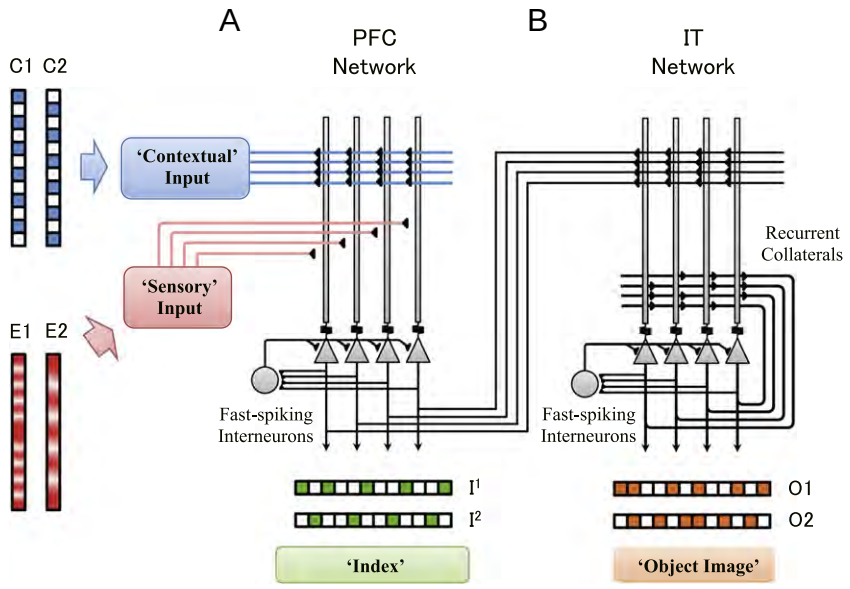

Fig. 3. Schematic diagram of the PFC and IT networks. (A) Network architecture of the PFC. The network consists of a population of pyramidal neurons, and fast-spiking GABAergic interneurons with contextual inputs and image inputs. (B) Network architecture of the IT. The network consists of a population of pyramidal neurons that are reciprocally connected by recurrent connections and fast-spiking GABAergic interneurons with index inputs from the PFC.

input (Bar, 2004; Tomita et al., 1999). Moreover, attentional biasing signals can be generated in the absence of any visual stimulation whatsoever (Bar, 2006; Kastner & Ungerleider, 2001). The basic question is how the IT can activate a relevant object representation solely from a top-down index provided by the PFC. From a computational standpoint, the basic question is on the nature of the index received from the OSK network discussed in Section 3.

Since little information is available for answering such a question, here we discuss two theoretical possibilities. The first possibility concerns the active role played by the attentional and phasic cholinergic projections onto the IT, which we discussed at ICCN 2013 (Fujii et al., 2014). Phasic (transient) cholinergic (ACh) projections from the nucleus basalis of Meynert (NBM) (Kanamaru et al., 2013; Parikh, Kozak, Martinez, & Sarter, 2007) facilitate the transition of the IT network from a transitory (quasi-attractor) state to an attractor state. Top-down attention may facilitate the transition of the IT dynamics to the attractor regime while the index from the PFC contributes to the jump into the specified attractor (Kanamaru et al., 2013; Tsukada, Yamaguti, & Tsuda, 2013). If this is indeed the case, the postulated index could be a small part of the OSK network dynamics in the PFC.

However, whether phasic cholinergic projections from the NBM take place (Parikh et al., 2007) in individuals with VH, is not known, since attention deficiency is known as one of the principal symptoms of DLB.

Another theoretical possibility, which we simulate in this work, does not rely on special cholinergic projections from the NBM. Instead, we postulate that the index provided by the semantic knowledge system reflects its global activity, that is, a binary-transformed spatial pattern of each identity. See Section 6 for details.

6. Computational model of visual hallucination

This section presents a computational model of RCVH. An overall structure of the present model is shown in Fig. 3; the model is a unidirectionally coupled system of two neural networks.

The PFC–IT interaction has been postulated to be bidirectional in that the two cortices may communicate as a process such as biased competition in object recognition (Desimone, 1998; Fink et al., 1996; Fink, Marshall, Halligan, & Dolan, 2000; Grill-Spector, 2003; Henderson & Hollingworth, 1999; Shimamura, 2000). However, our computational model is assumed to be a unidirectionally coupled system for the following reason. We simulate object recognition under the assumption that both Pathway I connecting OFC and the visual cortex (principal disorder), and the axonal fibers connecting the IT and visual cortex (complementary disorder), are "disturbed", even if only temporarily. Thus, as shown in Fig. 1, both the PFC and the IT cortex are essentially blind to the external object at the center of attention.

The PFC creates a hallucinatory index based solely on its own internal interpretation of context and expectancy. The IT implements this "false" index in a visual image. In a normal case, this IT process would, based on detailed bottom-up information from the visual cortex, be complemented by interactions with the PFC when necessary. In RCVH, this PFC–IT interaction is not expected to function as it would in a normal cognition process.

6.1. Model network for the prefrontal cortex

The first network is the model of the PFC, that is, the OSK network (Section 3), and the second is the model of the IT as the object representation network (Section 5).

The model PFC receives, among others, three kinds of signals from Pathways I, II, and III as explained above. Pathway I conveys images of the object at the center of attention (Bar, 2003) via long-distance connections from visual cortex, plus some random background noise. Pathway II conveys emotion and expectancy via the OFC-IT-Amygdala triad (Ghashghaei & Barbas, 2002), and Pathway III conveys the gist-based contextual information from the retrosplenial and parahippocampal cortices (Fenske et al., 2006). We lumped the three pathways into two, namely, Pathway I and Pathway II/III, for the sake of computational simplicity without losing the essence of the structure. Signals from Pathway I, namely, sensory inputs, play the role of reference input. Signals from Pathway II/III, namely, contextual inputs, are regarded as association inputs. The output guess (in the form of the index) from the PFC network is then sent to the IT as a top-down trigger to facilitate activation of the image of the "seen" object.

In the construction of the computational model, we adopted the Pinsky–Rinzel neuron model (Pinsky & Rinzel, 1994) for pyramidal

neurons and the Wang–Buzsáki model (Wang & Buzsáki, 1996) for fast-spiking interneurons (see Appendices A and B). The inputs are assumed to be conveyed by Poisson spike sequences with the alpha rhythm for contextual inputs and the gamma rhythm for sensory inputs.

We first constructed the PFC and IT models separately, and combined them to check their capability as a computational hallucinator.

Fig. 3 shows the PFC network (i.e., the OSK network). This network with N pyramidal neurons constitutes a hetero-associative network, associating contextual inputs with visual inputs. The network possesses plastic synaptic connections of contextual inputs to the pyramidal neurons in the presence of visual images as reference inputs, which may be a reflection of facilitation. We embedded "superimposed" hetero-association in the synaptic connections; in other words, we embedded multiple correspondence between context inputs and visual images. It should be noted that in conventional hetero-associative networks, only one-to-one correspondence between two kinds of patterns is formulated: each pair of corresponding different patterns, $(x^{(m)}, y^{(m)})$ $(m = 1, \ldots, M)$, is associated and embedded in synaptic connections for all pairs. On the other hand, in the present network, $M \times M$ pairs of different patterns, $(x^{(i)}, y^{(j)})$ $(i, j = 1, \ldots, M)$, are associated and embedded. Here, contextual inputs are encoded as binary patterns whereas gray scale levels representing means of real numbers are adopted for visual images.

Fig. 4 shows a typical example of the input–output relation, accompanying the internal dynamics of spike patterns. A pair consisting of context $C1$ and visual pattern $E1$ was input during some interval of time, and after that interval, only $C1$ was input; by inputting $C1$ only, we simulate visual information being lost by conduction disturbance due to damage to long-range fibers between the visual cortex and PFC (Pathway I). Spike sequences of outputs of pyramidal neurons are also shown in the form of raster plot.

The outputs of pyramidal neurons in the PFC–OSK network must convey index information expressing contextual facilitation caused by an association of complex information on context and visual images.

6.2. Index as a spatial pattern of identity

We introduced an auxiliary operation in the pyramidal neurons, namely, another threshold operation. For spike sequences during some time interval T_j, we calculated the number of spikes $x_i^{T_j}$ for neuron i. Let $\langle x_i^{T_j} \rangle$ be the time average of $x_i^{T_j}$. The proposed index for the output of neuron i is given by $I_i^{T_j} \equiv \theta(x_i^{T_j} - \langle x_i^{T_j} \rangle)$, where $\theta(z)$ is a Heaviside function: $\theta(z) = 1$ if $z > 0$ and otherwise $\theta(z) = 0$. A total index of the network during the interval T_j is expressed as a vector, $I^j \equiv (I_1^{T_j}, \ldots, I_N^{T_j})$.

Fig. 4 (D) shows the direction cosines of network outputs during T_1 and T_2, and the corresponding indices I^1 and I^2. During T_1 when both the contextual input $C1$ and the visual input $E1$ are provided, the network output shows a preference toward index I^1 over index I^2. On the other hand, during T_2 when only contextual input $C1$ is provided, the network output shows a preference toward index I^2 over I^1.

How does this change of index information in the PFC influence the output of the IT network? Let us construct a model network of the IT and study the network activity when the IT network receives inputs on index information.

6.3. Model network for IT—object representation network

For the IT, we constructed a network model, that is, the Object Representation Network. We presumed that this network would activate a visual representation of an image triggered by an index signal from PFC.

We present the architecture of our model, which consists two subnetworks. The main part is a recurrent network in which images of visual objects are built-in as attractors, say $O1$ and $O2$. Another part is a pre-processor (i.e., an interpreter for incoming indices) that is designed to be a hetero-associative network between indices and visual images of objects. In the present simulation, such hetero-associations are built-in *a priori*, but in the realistic brain such associations could be established via plasticity. Visual images of the objects, $O1$ and $O2$ are constructed by discretizing object images, $E1$ and $E2$, respectively, with a threshold of 0.8.

The assumption that the main network in the IT functions as an attractor network may stem from experimental observations on activity in visual memory task (by, e.g., Tomita et al., 1999). Furthermore, their observations suggest that IT neurons activate even without direct bottom-up visual information. Thus, it is plausible to consider that the IT reactivates visual images caused by only top-down signals—an index in the present paper.

Fig. 5 shows numerical results of the activation of visual images of objects triggered by the index resulting from PFC outputs. During the interval when the PFC receives both the contextual input $C1$ and the visual image $E1$, the IT produces a clear object image $O1$ corresponding to $E1$. On the other hand, during the interval when the PFC receives the contextual input $C1$ alone, which implies a deficit of visual information, the IT produces another object image $O2$. The production of $O2$ is due to the association with $C1$, but this contextual information could be incorrect.

Thus, this numerical result implies the possibility that disturbances of visual information in the PFC brings about a "false" index for the object, which then gives rise to evocation of a mismatched visual object image in the IT. This kind of mismatched image in the IT may be one of the key mechanisms of VH in DLB.

7. Summary and discussions

In this paper, we proposed a computational model of the PFC–IT complex to elucidate the neural mechanism of RCVH in DLB. Simulation results suggest the possibility that deficits of visual information in the PFC bring about a hallucinatory index, which in turn cause the production of a mismatched visual object image in the IT.

As stated in Section 4, the hallucinations in DLB may occur due to the two disconnection events, the principal and complementary disorders. The PFC–VLPFC and OFC are involved in the first disconnections, while the IT is related to the second one. The three pathways related to the principal disorder convey signals to the PFC and are all critical in the decision of identity. Of these three, only Pathway I is hypothesized to be damaged, while Pathways II and III appear intact. This may give an account for the seemingly strange symptomatology of VH in DLB introduced in Section 1.

In other words, the key point is the role of intact indices for top-down biasing in the prefrontal–inferior temporal interacting system that is disconnected from sensory inputs.
We emphasize that the index system in the PFC may be intact, but the PFC is disconnected from sensory inputs.

As other theoretical frameworks that look similar to top-down facilitation, one may consider the following two theories: Convergence Divergence Zone (CDZ) theory (Damasio, 1989; Meyer & Damasio, 2009), and Hierarchical Dynamical Models (HDMs) theory (Friston, 2008; Friston & Kiebel, 2009). However, the CDZ theory does not include the cortical "shortcut" such as the Pathway I, which is a core structure to produce RCVH in DLB in the present theory. Furthermore, with the CDZ theory, it would be quite difficult to elucidate the neural mechanism of Hallucinatory images that are additionally superimposed on a normal background scene, only at the center of attention. On the other hand, the HDMs theory

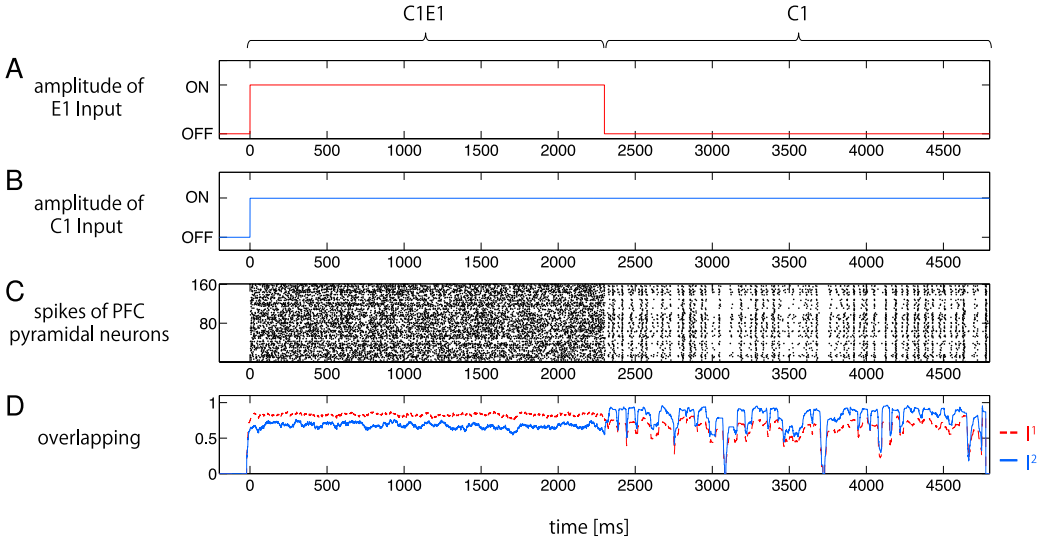

Fig. 4. Effect of conduction disturbances in PFC. (A) Time sequence of the amplitude of image inputs. Inputs were applied to each cell assembly at time 0 ms, and stopped at time 2250 ms. (B) Time sequence of the amplitude of contextual inputs. The inputs were applied to each cell assembly at time 0 ms, and supplied until the end of the simulation. (C) Raster plot of pyramidal neurons in the PFC network. (D) Overlapping between current activity of PFC pyramidal neurons and index patterns. Different colors indicate different indices (red dotted line: I^1; blue solid line: I^2). The network received C1 and E1 between $t = 0$ and 2250 ms, and E1 was turned off at $t = 2250$ ms.

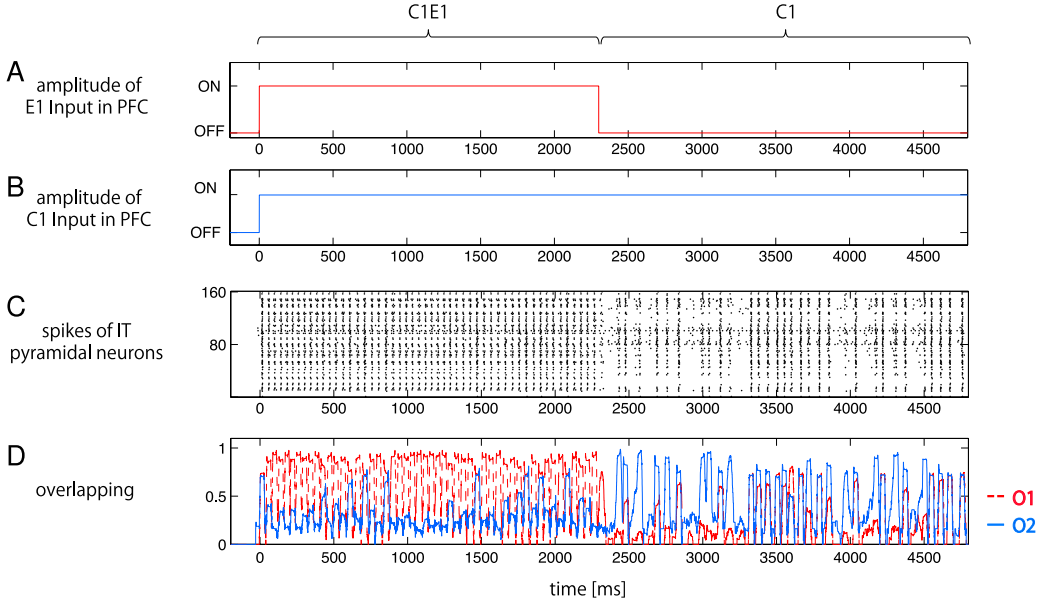

Fig. 5. Effect of conduction disturbances in the IT. (A) Time sequence of amplitude of the image inputs in the PFC. (B) Time sequence of the amplitude of contextual inputs in the PFC. (C) Raster plots of IT pyramidal neurons. (D) Overlapping between current activity of IT pyramidal neurons and patterns of object images. Different colors indicate different object images (red dotted line: O1; blue solid line: O2).

refers to the prediction error in perception. Although the prediction error plays an essential role in any perception including hallucinations, it does not directly refer to the mechanism of RCVH in DLB. However, the somatic maker hypothesis by Damasio (1994) and the predictive coding hypothesis by Friston (2005, 2008) and Friston and Kiebel (2009) might be related to the process of the production of "index" in prefrontal cortex. In this respect, both theories will be helpful to develop the theory of complex visual hallucinations that we described in this paper.

Other important characteristics of RCVH introduced in Section 1 are, however, beyond the scope of the present model. For instance, the model does not address the relationship between RCVH in DLB and decreased cholinergic activity in the cortex (Collerton et al., 2005). The decrease in cortical and subcortical cholinergic levels (see, Kanamaru et al., 2013) may bring about attention deficit, but its causal relationship with RCVH is not well understood. Also, the neural mechanism of the long-term persistence of hallucinatory images lasting up to a few minutes is not well understood, and probably does not fall within the framework of conduction disturbances. It should also be noted that the spontaneous persistence time of VH is most frequently a few minutes, but it possesses a distribution from seconds to hours (Mosimann et al., 2006). The long-term persistent of VH might arise from dynamic interactions between the PFC and IT (Shimamura, 2000), regulated by neuromodulators such as dopamine and acetylcholine. However, no report has been published that clearly shows its neural mechanism.

Another interesting phenomenon in the retention of VH has been reported: VH suddenly disappears when correct contextual

information is provided (See, for example, http://www.nhk.or.jp/gatten/). Thus, VH in DLB seems to be specifically and dynamically associated with contextual information.

In this paper, we examined the hypothesis that when some connections (or brain fasciculi) between the PFC and visual cortex are lost due to conduction disturbance, the PFC produces a false index and hence the IT inevitably activates a wrong image. This result is the first step toward gaining an integrated view of RCVH in DLB. A unified theory remains a topic for future study.

Acknowledgments

We would like to express our special thanks to Daniel Collerton for valuable discussions and offering a number of critical improvements on RCVH of DLB. Thanks are also due to Guy Sandner and Yuichi Katori for their valuable discussions. The first, second and fourth authors (HT, HF, and IT) were supported by a Grant-in-Aid for Scientific Research on Innovative Areas (No. 4103) (21120002) from Ministry of Education, Culture, Sports, Science and Technology (MEXT) in Japan, and partially supported by Human Frontier Science Program Organization (HFSP:RGP0039).

Appendix A. Pyramidal neurons

We employ the two-compartment model for pyramidal neurons that was proposed by Pinsky and Rinzel (1994) for both the PFC and the IT. The model consists of somatic and dendritic compartments comprising different active ion-currents and synaptic inputs.

The membrane potentials of each compartment are given by

$$\begin{aligned} C_m\frac{dV_s}{dt} &= -g_{\mathrm{L}}(V_s-E_{\mathrm{L}})-I_{\mathrm{Na}}-I_{K-\mathrm{DR}}-I^s_{\mathrm{syn}} \\ &\quad +(g_c/p)(V_d-V_s)+I_s/p, \\ C_m\frac{dV_d}{dt} &= -g_{\mathrm{L}}(V_d-E_{\mathrm{L}})-I_{\mathrm{Ca}}-I_{K-\mathrm{AHP}}-I_{K-C} \\ &\quad -I^d_{\mathrm{syn}}/(1-p)+(g_c/(1-p))(V_s-V_d) \\ &\quad +I_d/(1-p), \end{aligned} \tag{A.1}$$

where I_{Na} and $I_{K-\mathrm{DR}}$ in the somatic compartment are the fast sodium current and the delayed rectifier potassium current, respectively. I_{Ca}, I_{K-C}, and $I_{K-\mathrm{AHP}}$ in the dendritic compartment are the calcium current, the Ca-activated potassium current, and the potassium after-hyperpolarization current, respectively. The compartments are electrically connected via conductance g_c, and p is the percentage of soma compartment area. The ionic currents are given by

$$\begin{aligned} I_{\mathrm{Na}} &= g_{\mathrm{Na}}m^2_\infty h(V_s-E_{\mathrm{Na}}), \\ I_{K-\mathrm{DR}} &= g_{K-\mathrm{DR}}n(V_s-E_{\mathrm{K}}), \\ I_{\mathrm{Ca}} &= g_{\mathrm{Ca}}s^2(V_d-E_{\mathrm{Ca}}), \\ I_{K-\mathrm{AHP}} &= g_{K-\mathrm{AHP}}q(V_d-E_{\mathrm{K}}), \\ I_{K-C} &= g_{K-C}c\,\min(\mathrm{Ca}/250,\ 1)(V_d-E_{\mathrm{K}}). \end{aligned} \tag{A.2}$$

The kinetics of gating variables are described by

$$\frac{dx}{dt}=\varphi(\alpha_x(1-x)-\beta_x x), \tag{A.3}$$

where x denotes the different kinetic variables h, n, m, s, and q. α_x and β_x are the rate functions of channel opening and closing, and φ tunes the time scale of the rate.

$$\begin{aligned} \alpha_m &= \frac{0.32(-46.9-V_s)}{\exp((-46.9-V_s)/4)-1}, \\ \beta_m &= \frac{0.28(V_s+19.9)}{\exp((V_s+19.9)/5)-1}, \\ \alpha_n &= \frac{0.016(-24.9-V_s)}{\exp((-24.9-V_s)/5)-1}, \\ \beta_n &= 0.25\exp(-1-0.025V_s), \\ \alpha_h &= 0.128\exp((-43-V_s)/18), \\ \beta_h &= \frac{4}{1+\exp((-20-V_s)/5)}, \\ \alpha_s &= \frac{1.6}{1+\exp(-0.072(V_d-5))}, \\ \beta_s &= \frac{0.02(V_d+8.9)}{\exp((V_d+8.9)/5)-1}, \\ \alpha_q &= 0.01\,\min(\mathrm{Ca}/500,\ 1), \qquad \beta_q = 0.001, \\ \alpha_c &= \begin{cases} \dfrac{\exp((V_d+50)/11)-\exp((V_d+53.5)/27)}{18.975} & \\ \quad V_d\le -10, & \\ 2\exp((V_d+53.5)/27) & V_d>-10, \end{cases} \\ \beta_c &= \begin{cases} 2\exp((V_d+53.5)/27)-\alpha_c & V_d\le -10, \\ 0 & V_d>-10. \end{cases} \end{aligned} \tag{A.4}$$

The kinetic variable m was approximated by its asymptotic value:

$$m_\infty=\frac{\alpha_m}{\alpha_m+\beta_m}. \tag{A.5}$$

The calcium concentration Ca satisfies

$$\frac{d\mathrm{Ca}}{dt}=-0.13I_{\mathrm{Ca}}-0.075\ \mathrm{Ca}. \tag{A.6}$$

The synaptic current I^s_{syn} and I^d_{syn} are defined below (see Appendix C). We used the following standard values for the parameters of the pyramidal neuron. The maximal conductances (in mS/cm^2) were $g_c=2.1$, $g_{\mathrm{Na}}=30$, $g_{K-\mathrm{DR}}=25$, $g_{\mathrm{L}}=0.1$, $g_{\mathrm{Ca}}=2.5$, $g_{K-\mathrm{AHP}}=0.8$, and $g_{K-C}=15$. The reversal potentials (in mV) were $E_{\mathrm{K}}=-75$, $E_{\mathrm{Na}}=60$, $E_{\mathrm{Ca}}=80$, and $E_{\mathrm{L}}=-60$. The applied currents (in μA/cm^2) were $I_s=-0.5$, $I_d=0$. The capacitance was $C_m=3\,\mu$F/cm^2, the time scale was $\varphi=1$, and the proportion of soma area was $p=0.5$.

Appendix B. Fast-spiking GABAergic interneurons

We employ the Wang–Buzsáki model (Wang & Buzsáki, 1996) for the interneurons, which is a single compartment model with sodium and potassium channels. The equation for the potential is

$$C_m\frac{dV}{dt}=-I_{\mathrm{Na}}-I_{\mathrm{K}}-I_{\mathrm{L}}-I^{fs}_{\mathrm{syn}}+I_{fs}, \tag{B.1}$$

where I_{Na}, I_{K}, and I_{L} are the sodium, potassium, and leak current, respectively. I_{fs} is the constant current. The ionic currents are given by

$$\begin{aligned} I_{\mathrm{Na}} &= g_{\mathrm{Na}}m^3_\infty h(V-E_{\mathrm{Na}}), \\ I_{\mathrm{K}} &= g_{\mathrm{K}}n^4(V-E_{\mathrm{K}}), \\ I_{\mathrm{L}} &= g_{\mathrm{L}}(V-E_{\mathrm{L}}). \end{aligned} \tag{B.2}$$

The kinetic variables h and n obey Eq. (A.3), and m obeys Eq. (A.5). The rate constants are given by

$$\begin{aligned}
\alpha_m &= \frac{-0.1(V+35)}{\exp(-0.1(V+35))-1},\\
\beta_m &= 4\exp(-(V+60)/18),\\
\alpha_h &= 0.07\exp(-(V+58)/20),\\
\beta_h &= \frac{1}{\exp(-0.1(V+28))+1},\\
\alpha_n &= \frac{-0.01(V+34)}{\exp(-0.1(V+34))-1},\\
\beta_n &= 0.125\exp(-(V+44)/80).
\end{aligned} \tag{B.3}$$

We used the following standard values for the parameters of interneurons. The maximal conductances (in mS/cm^2) were $g_{\mathrm{Na}} = 35$, $g_{\mathrm{K}} = 9$, and $g_{\mathrm{L}} = 0.1$. The reversal potentials were $E_{\mathrm{Na}} = 55$, $E_{\mathrm{K}} = -90$, and $E_{\mathrm{L}} = -65$. Other parameters were $C_m = 1$, $\varphi = 5$, and $I_{fs} = 0$.

Appendix C. Synaptic connections

The synaptic currents for the PFC networks are given by

$$\begin{aligned}
I^d_{\mathrm{syn}} &= I_C + I_E + I_{ne},\\
I^s_{\mathrm{syn}} &= I_{ie},\\
I^{fs}_{\mathrm{syn}} &= I_{ei} + I_{ni},
\end{aligned} \tag{C.1}$$

where

$$\begin{aligned}
I_C &= \left(g_C^{\mathrm{AMPA}}\sum_{j=1}^{N_e} w_j^{\mathrm{PFC}} s_j^{\mathrm{AMPA},C} + g_C^{\mathrm{NMDA}}\sum_{j=1}^{N_e} w_j^{\mathrm{PFC}} s_j^{\mathrm{NMDA},C}\right.\\
&\quad\left.\times(1+0.28\exp(-0.062V))^{-1}\right)(V-E_{\mathrm{syn}}),\\
I_E &= \left(g_E^{\mathrm{AMPA}} e^{(m)} s^{\mathrm{AMPA},E} + g_E^{\mathrm{NMDA}} e^{(m)} s^{\mathrm{NMDA},E}\right.\\
&\quad\left.\times(1+0.28\exp(-0.062V))^{-1}\right)(V-E_{\mathrm{syn}}),\\
I_{ei} &= g_{ei}\sum_{j=1}^{N_e} w_j^{ei} s_j^{ei}(V-E_{\mathrm{syn}}),\\
I_{ne} &= \left(g_{ne}^{\mathrm{AMPA}} s^{\mathrm{AMPA},ne} + g_{ne}^{\mathrm{NMDA}} s^{\mathrm{NMDA},ne}\right.\\
&\quad\left.\times(1+0.28\exp(-0.062V))^{-1}\right)(V-E_{\mathrm{syn}}),\\
I_{ni} &= g_{ni} s^{ni}(V-E_{\mathrm{syn}}),\\
I_{ie} &= g_{ie}\sum_{j=1}^{N_i} w_j^{ie} s_j^{ie}(V-E_{\mathrm{GABA}}).
\end{aligned} \tag{C.2}$$

Here I_C, I_E, and I_N (N denotes ne and ni) are synaptic currents of a contextual input, a sensory input, and a noise input, respectively. I_{ei} and I_{ie} are synaptic currents from pyramidal neuron to interneuron, and from interneuron to pyramidal neuron, respectively. V is a membrane potential, and s_j is a kinetic variable labeled by the index j of a presynaptic neuron. $e^{(m)}$ is the mth sensory input pattern, and assumed to be uniformly distributed between 0 and 1. The parameter values of conductance (in mS/cm^2) for the PFC simulation are $g_C^{\mathrm{AMPA}} = 0.03$, $g_C^{\mathrm{NMDA}} = 0$, $g_E^{\mathrm{AMPA}} = 1$, $g_E^{\mathrm{NMDA}} = 0$, $g_{ei} = 0.05$, $g_{ne}^{\mathrm{AMPA}} = 0.005$, $g_{ne}^{\mathrm{NMDA}} = 0$, $g_{ni} = 0.01$, and $g_{ie} = 0.03$. The reversal potentials (in mV) are $E_{\mathrm{syn}} = 0$, $E_{\mathrm{GABA}} = -75$.

The synaptic currents for the IT networks are given by

$$\begin{aligned}
I^d_{\mathrm{syn}} &= I_{\mathrm{rec}} + I_I + I_{ne},\\
I^s_{\mathrm{syn}} &= I_{ie},\\
I^{fs}_{\mathrm{syn}} &= I_{ei} + I_{ni},
\end{aligned} \tag{C.3}$$

where

$$\begin{aligned}
I_I &= \left(g_I^{\mathrm{AMPA}}\sum_{j=1}^{N_e} w_j^{\mathrm{IT},I} s_j^{\mathrm{AMPA},I} + g_I^{\mathrm{NMDA}}\sum_{j=1}^{N_e} w_j^{\mathrm{IT},I} s_j^{\mathrm{NMDA},I}\right.\\
&\quad\left.\times(1+0.28\exp(-0.062V))^{-1}\right)(V-E_{\mathrm{syn}}),\\
I_{\mathrm{rec}} &= \left(g_{\mathrm{rec}}^{\mathrm{AMPA}}\sum_{j=1}^{N_e} w_j^{\mathrm{IT,rec}} s_j^{\mathrm{AMPA,rec}}\right.\\
&\quad + g_{\mathrm{rec}}^{\mathrm{NMDA}}\sum_{j=1}^{N_e} w_j^{\mathrm{IT,rec}} s_j^{\mathrm{NMDA,rec}}\\
&\quad\left.\times\ (1+0.28\exp(-0.062V))^{-1}\right)(V-E_{\mathrm{syn}}).
\end{aligned} \tag{C.4}$$

Here I_I and I_{rec} are a synaptic current of the index from the PFC, and recurrent collateral from other pyramidal neurons in the IT. I_{ei}, I_{ie}, and I_N (N denotes ne and ni) are the same equations as Eq. (C.2). The parameter values of conductance (in mS/cm^2) for the IT simulation are $g_I^{\mathrm{AMPA}} = 0.0045$, $g_I^{\mathrm{NMDA}} = 0.0072$, $g_{\mathrm{rec}}^{\mathrm{AMPA}} = 0.02$, $g_{\mathrm{rec}}^{\mathrm{NMDA}} = 0.032$, and $g_{ie} = 0.11$. Other parameters g_{ei}, g_{ne}^{AMPA}, g_{ne}^{NMDA}, g_{ni}, E_{syn}, and E_{GABA} have the same values as in the PFC simulation.

The connection matrices were determined in the following way. Each component of the connection matrix w^{ei} from pyramidal neurons to interneurons takes a value of 1 or 0. Each interneuron receives synaptic inputs from four pyramidal neurons, which are chosen randomly from the whole pyramidal neuron population. The elements of the connection matrix w^{ie} from interneurons to pyramidal neurons are assumed to be uniformly distributed between 0 and 1.

The synaptic strength w_{ij}^{PFC} is given by

$$w_{ij}^{\mathrm{PFC}} = \sum_{m,n=1}^{M} x_i^{(m)} y_j^{(n)} \quad (m,n=1,\ldots,M), \tag{C.5}$$

where $x_i^{(m)}$ is the ith component in the mth contextual input pattern, and $y_j^{(n)}$ is the jth component in the nth sensory input pattern in the PFC.

The dendritic compartments of IT neurons receive the spike trains from the PFC neurons. The synaptic strength $w_{ij}^{\mathrm{IT},I}$ is given by

$$w_{ij}^{\mathrm{IT},I} = \sum_{m=1}^{M} x_i^{(m)} y_j^{(m)} \quad (m=1,\ldots,M), \tag{C.6}$$

where $x_i^{(m)}$ is the ith component in the mth index pattern, and $y_j^{(m)}$ is the jth component in the mth object image. We assumed $M = 2$ for both the PFC and IT simulations for simplicity.

Two object images are embedded into the recurrent excitatory synaptic connections by Hebbian synaptic modification. The Hebbian rule specifies a weight of 1 for a connection between two active neurons, and a weight of 0 otherwise:

$$w_{ij}^{\mathrm{IT,rec}} = \Theta\left(\sum_{m=1}^{M} y_i^{(m)} y_j^{(m)}\right), \qquad \Theta(x) = \begin{cases} 1 & (x>0),\\ 0 & (x\le 0), \end{cases} \tag{C.7}$$

where $y_i^{(m)}$ is the ith component in the mth object image, each of which is encoded by the value 1 (firing state) or 0 (resting state). These weight matrices w_{ij}^{PFC}, $w_{ij}^{\mathrm{IT},I}$, and $w_{ij}^{\mathrm{IT,rec}}$ are fixed during simulation.

The synaptic gating variables for the AMPA and NMDA synapses obey

$$\frac{ds^{\mathrm{AMPA}}}{dt} = \Theta(V_{\mathrm{pre}}+40) - \beta_A s^{\mathrm{AMPA}}, \tag{C.8}$$

$$\frac{ds^{\mathrm{NMDA}}}{dt} = \Theta(V_{\mathrm{pre}}+50) - \beta_N s^{\mathrm{NMDA}}, \tag{C.9}$$

where V_{pre} is the presynaptic potential, and $\beta_A = 0.5\,\text{ms}^{-1}$ and $\beta_N = 0.0067\,\text{ms}^{-1}$ are decay rates.

The synaptic gating variables, $s^{X,C}$, $s^{X,E}$, $s^{X,ne}$, and s^{ni} (X denotes AMPA and NMDA), obey

$$\frac{ds}{dt} = \sum_k \delta(t - t^k_{\text{Poisson}}) - \beta_e s, \tag{C.10}$$

where t^k_{Poisson} is the time of the kth spike in a Poisson spike train. Each spike train is independently generated by a Poisson process with an average firing rate of 12 Hz for contextual inputs, 40 Hz for sensory inputs, and 1 kHz for background noise.

The synaptic gating variable s^{ie} obeys

$$\begin{aligned} &\frac{ds}{dt} = \alpha_i F(V_{\text{pre}})(1 - s) - \beta_i s, \\ &F(V_{\text{pre}}) = 1/(\exp(-V_{\text{pre}}/2) + 1), \end{aligned} \tag{C.11}$$

where $\alpha_i = 12\,\text{ms}^{-1}$ and $\beta_i = 0.1\,\text{ms}^{-1}$ are the rise and decay rates for the inhibition of pyramidal neurons.

The PFC and IT networks are composed of 200 neurons, respectively: 160 pyramidal neurons (80%) and 40 interneurons (20%). GABAergic interneurons project via $GABA_A$ synapse to the somatic compartment of pyramidal neurons, and the pyramidal neurons project via AMPA synapses to interneurons. Numerical integration was performed by a fourth-order Runge–Kutta method using a 0.05 ms time step.

Appendix D. Calculation of overlapping

We defined a degree of memory retrieval by calculating the overlapping M^μ between the reference pattern (e.g., index, object image) and the current network state. The overlapping is defined by

$$M^\mu(t) = \frac{\eta^\mu \cdot X^{\Delta t}(t)}{\|\eta^\mu\| \left\|X^{\Delta t}(t)\right\|}, \tag{D.1}$$

where η^μ is the μth reference pattern, and $X^{\Delta t}(t)$ is an N-dimensional vector for an N-neuron network:

$$X^{\Delta t}(t) = \left(x_1^{\Delta t}(t), x_2^{\Delta t}(t), \ldots, x_N^{\Delta t}(t)\right). \tag{D.2}$$

Here $x_i^{\Delta t}(t)$ is the number of spikes of the ith neuron during the interval $(t + \Delta t)$ and $\Delta t = 50$ ms is fixed.

References

Bar, M. (2003). A cortical mechanism for triggering top-down facilitation in visual object recognition. *Journal of Cognitive Neuroscience*, *15*, 600–609.

Bar, M. (2004). Visual objects in context. *Nature Reviews Neuroscience*, *5*, 617–629.

Bar, M. (2006). Top-down facilitation of visual recognition. *Proceedings of the National Academy of Sciences*, *103*, 449–454.

Biederman, I., Rabinowitz, J., Glass, A. L., & Stacy, E. W., Jr. (1974). On the information extracted from a glance at a scene. *Journal of Experimental Psychology*, *103*, 597–600.

Catani, M., & de Schotten, M. T. (2012). *Atlas of human brain connections*. Oxford University Press.

Catani, D., & ffytche, D. H. (2005). The rises and falls of disconnection syndromes. *Brain*, *128*, 2224–2239.

Chaumon, M., Kveraga, K., Barrett, L. F., & Bar, M. (2013). Visual predictions in the orbitofrontal cortex rely on associative content. *Cerebral Cortex*, http://dx.doi.org/10.1093/cercor/bht146.

Collerton, D., Dudley, R., & Mosimann, U. P. (2012). Visual hallucinations. In J. D. Blom, & I. E. C. Sommer (Eds.), *Hallucinations. Research and practice* (pp. 75–90). New York, NY: Springer.

Collerton, D., Perry, E., & McKeith, I. (2005). Why people see things that are not there: a novel perception and Attention Deficit model for recurrent complex visual hallucinations. *Behavioral and Brain Sciences*, *28*, 737–794.

Court, J. A., Ballard, C. G., Piggott, M. A., Johnson, M., O'Brien, J. T., Holmes, C., et al. (2001). Visual hallucinations are associated with lower α bungarotoxin binding in dementia with Lewy bodies. *Pharmacology Biochemistry and Behavior*, *70*, 571–579.

Damasio, A. R. (1989). Time-locked multiregional retroactivation: a systems-level proposal for the neural substrates of recall and recognition. *Cognition*, *33*, 25–62.

Damasio, A. R. (1994). *Descartes' error: emotion, reason, and the human brain*. New York: Grosset/Putnam.

Desimone, R. (1998). Visual attention mediated by biased competition in extrastriate visual cortex. *Philosophical Transactions of the Royal Society of London, Series B*, *353*, 1245–1255.

Epstein, R., & Kanwisher, N. (1998). A cortical representation of the local visual environment. *Nature*, *392*, 598–601.

Fenske, M. J., Aminoff, E., Gronau, N., & Bar, M. (2006). Top-down facilitation of visual object recognition: object-based and context-based contributions. *Progress in Brain Research*, *155*, 3–21.

ffytche, D. H. (2008). The hodology of hallucinations. *Cortex*, *44*, 1067–1083.

Fink, G. R., Halligan, P. W., Marshall, J. C., Frith, C. D., Frackowiak, R. S., & Dolan, R. J. (1996). Where in the brain does visual attention select the forest and the trees? *Nature*, *382*, 626–628.

Fink, G. R., Marshall, J. C., Halligan, P. W., & Dolan, R. J. (2000). Neuronal activity in early visual areas during global and local processing: a comment on Heinze, Hinrichs, Scholz, Burchert and Mangun. *Journal of Cognitive Neuroscience*, *12*, 355–356.

Friston, K. J. (2005). A theory of cortical responses. *Philosophical Transactions of the Royal Society of London, Series B: Biological Sciences*, *360*, 815–836.

Friston, K. J. (2008). Hierarchical models in the brain. *PLoS Computational Biology*, *4*, e1000211.

Friston, K. J., & Kiebel, S. J. (2009). Predictive coding under the free-energy principle. *Philosophical Transactions of the Royal Society of London, Series B: Biological Sciences*, *264*, 1211–1221.

Fujii, H., Tsukada, H., Tsuda, I., & Aihara, K. (2014). Visual hallucinations in dementia with lewy bodies (I): a hodological view. In H. Liljenstrom (Ed.), *Advances in cognitive neurodynamics (IV)—proceedings of the international conference on cognitive neurodynamics (ICCN) 2013*. Springer-Verlag.

Geshwind, N. (1965). Disconnexion syndromes in animals and man. Part I. *Brain*, *88*, 237–294;
Geshwind, N. (1965). Disconnexion syndromes in animals and man. Part II. *Brain*, *88*, 585–643.

Ghashghaei, H. T., & Barbas, H. (2002). Pathways for emotion: interaction of prefrontal and anterior temporal pathways in the amygdala of the rhesus monkey. *Neuroscience*, *115*, 1261–1279.

Goedert, M., Spillantini, M. G., Del Tredici, K., & Braak, H. (2013). 100 years of Lewy pathology. *Nature Reviews Neurology*, *9*, 13–24.

Grill-Spector, K. (2003). The neural basis of object perception. *Current Opinion in Neurobiology*, *13*, 159–166.

Henderson, J. M., & Hollingworth, A. (1999). High-level scene perception. *Annual Review of Psychology*, *50*, 243–271.

Kanamaru, T., Fujii, H., & Aihara, K. (2013). Deformation of attractor landscape via cholinergic presynaptic modulations: a computational study using a phase neuron model. *PLoS One*, *8*, e53854.

Kastner, S., & Ungerleider, L. G. (2001). The neural basis of biased competition in human visual cortex. *Neuropsychologia*, *39*, 1263–1276.

Kiuchi, K., Morikawa, M., Taoka, T., Kitamura, S., Nagashima, T., Makinodan, M., et al. (2011). White matter changes in dementia with Lewy bodies and Alzheimer's disease: a tractography-based study. *Journal of Psychiatric Research*, *45*, 1095–1100.

Kveraga, K., Ghuman, A. S., & Bar, M. (2007). Top-down predictions in the cognitive brain. *Brain and Cognition*, *65*, 145–168.

Lichtheim, L. (1885). On aphasia. *Brain*, *7*, 433–484.

McKeith, I. G., Dickson, D. W., Lowe, J., Emre, M., O'Brien, J. T., Feldman, H., et al. (2005). Diagnosis and management of dementia with Lewy bodies: third report of the DLB consortium. *Neurology*, *65*, 1863–1872.

Meyer, K., & Damasio, A. R. (2009). Convergence and divergence in a neural architecture for recognition and memory. *Trends in Neurosciences*, *32*, 376–382.

Mosimann, U. P., Rowan, E. N., Partington, C. E., Collerton, D., Littlewood, E., O'Brien, J. T., et al. (2006). Characteristics of visual hallucinations in Parkinson disease dementia and dementia with lewy bodies. *The American Journal of Geriatric Psychiatry*, *14*, 153–160.

Ota, M., Sato, N., Ogawa, M., Murata, M., Kuno, S., Kida, J., et al. (2009). Degeneration of dementia with Lewy bodies measured by diffusion tensor imaging. *NMR in Biomedicine*, *22*, 280–284.

Parikh, V., Kozak, R., Martinez, V., & Sarter, M. (2007). Prefrontal acetylcholine release controls cue detection on multiple timescales. *Neuron*, *56*, 141–154.

Perry, E. K., & Perry, R. H. (1995). Acetylcholine and hallucinatiaons: desease related compared to drug-induced alterations in human consciousness. *Brain and Cognition*, *28*, 240–258.

Pinsky, P. F., & Rinzel, J. (1994). Intrinsic and network rhythmogenesis in a reduced Traub model for CA3 neurons. *Journal of Computational Neuroscience*, *1*, 39–60.

Reid, R. T., Sabbagh, M. N., Corey-Bloom, J., Tiraboschi, P., & Thal, L. J. (2000). Nicotinic receptor losses in dementia with Lewy bodies: comparisons with Alzheimer's disease. *Neurobiology of Aging*, *21*, 741–746.

Rykhlevskaia, E., Uddin, L. Q., Kondos, L., & Menon, V. (2009). Neuroanatomical correlates of developmental dyscalculia: combined evidence from morphometry and tractography. *Frontiers in Human Neuroscience*, *3*, 1–13.

Sanchez-Castaneda, C., Rene, R., Ramirez-Ruiz, B., Campdelacreu, J., Gascon, J., Falcon, C., et al. (2010). Frontal and associative visual areas related to visual hallucinations in dementia with lewy bodies and Parkinson's disease with dementia. *Movement Disorders*, *25*, 615–622.

Sarubbo, S., De Benedictis, A., Maldonado, I. L., Basso, G., & Duffau, H. (2013). Frontal terminations for the inferior fronto-occipital fascicle: anatomical dissection, DTI study and functional considerations on a multi-component bundle. *Brain Structure and Function*, *218*, 21–37.

See, for example. http://www.nhk.or.jp/gatten/.

Shimamura, A. P. (2000). The role of the prefrontal cortex in dynamic filtering. *Psychobiology*, *28*, 207–218.

Summerfield, C., & Egner, T. (2009). Expectation (and attention) in visual cognition. *Trends in Cognitive Sciences*, *13*, 403–409.

Thiebaut de Schotten, M., Urbanski, M., Valabregue, R., Bayle, D. J., & Volle, E. (2012). Subdivision of the occipital lobes: an anatomical and functional MRI connectivity study. *Cortex*, http://dx.doi.org/10.1016/j.cortex.2012.12.007.

Tomita, H., Ohbayashi, M., Nakahara, K., Hasegawa, I., & Miyashita, Y. (1999). Top-down signal from prefrontal cortex in executive control of memory retrieval. *Nature*, *401*, 699–703.

Tsukada, H., Fujii, H., Tsuda, I., & Aihara, K. (2014). Visual hallucinations in dementia with lewy bodies (II): computational aspects. In H. Liljenstrom (Ed.), *Advances in cognitive neurodynamics (IV)—proceedings of the international conference on cognitive neurodynamics (ICCN) 2013*. Springer-Verlag.

Tsukada, H., Yamaguti, Y., & Tsuda, I. (2013). Transitory memory retrieval in a biologically plausible neural network model. *Cognitive Neurodynamics*, *7*, 409–416.

Wang, X. J., & Buzsáki, G. (1996). Gamma oscillation by synaptic inhibition in a hippocampal interneuronal network model. *The Journal of Neuroscience*, *16*, 6402–6413.